Spatial confinement of percolation: Monte Carlo modeling and nanoscale laser polymerization

A. Pikulin and N. Bityurin*
Institute of Applied Physics, RAS, 603950 Nizhniy Novgorod, Russia
(Received 30 April 2010; revised manuscript received 6 July 2010; published 4 August 2010)

Modern laser nanoprocessing technology employs the sharp, thresholdlike response of modified materials to laser exposure to create nanofeatures with sizes that are smaller than the diffraction limit. In this paper, the percolation transition is examined as a possible physical mechanism that allows such a nonlinear spatial confinement of the laser material alteration. In particular, the percolationlike transition is involved in laser polymerization techniques, including two-photon polymerization, which is capable of producing three-dimensional nanostructures with sizes of 100 nm and smaller. We perform Monte Carlo modeling of percolation with the spherically symmetric occupation probability distribution that is constrained in three dimensions. The dramatic increase in the fluctuations of the size and position of the largest connected cluster is observed when attempting to decrease its size below the critical scale. For laser polymerization, this provides the natural fluctuation-managed limitation of the minimal size of a nanofeature. We present a model that allows the analytical estimation of the critical size of the largest cluster. This analytical model fits well with the data obtained from the numerical experiments.

DOI: 10.1103/PhysRevB.82.085406 PACS number(s): 81.07.−b, 05.40.−a, 82.35.−x

I. INTRODUCTION

The laser micromodification and nanomodification of materials is broadly used for the creation of nanostructures both on the surface and within the bulk.[1] The modification mechanisms include ablation,[1,2] swelling,[3–7] melting,[8,9] multiphoton photochemistry,[10–12] local femtosecond laser dielectric breakdown,[13] etc. With a tightly focused laser beam, the direct writing of the complex structures with submicron resolution is possible, both in two and three dimensions. In most cases, the complex microstructures are typically made from thousands of elements, i.e., nanofeatures. The reduction in the size of an element allows the detailed elaboration of smaller structures. Such miniaturization is important for numerous applications.[8]

A way to minimize the size of the elementary structure is by employing the localization of the energy deposition within the smallest area. The minimum size of the laser spot is determined first by light diffraction. Further confinement of the energy deposition can be provided by the nonlinear absorption of the light energy due to coherent multiphoton transitions within the media, and/or light-induced, or thermally induced generation of absorbing species during the laser pulse.[2] However, even at the fixed spatial distribution of the deposited energy, phase transitions (evaporation/ablation, melting), or some other thresholdlike phenomena within the irradiated region, can provide the spatial localization of material modification at scales that are significantly smaller than the size of the energy deposition domain. Figure 1 shows that by decreasing the magnitude of energy deposition distribution just above the threshold, one can anticipate obtaining an arbitrary small size for the modified domain. An approach suggesting the significant decrease in the size of the structures below the diffraction limit by applying the laser power just slightly above the threshold was considered, for instance, in detail and employed in Refs. 14 and 15.

When investigating the problem of the localized light-induced material alteration, nonlocal processes such as heat or mass transfer (diffusion) are usually considered as factors that compete with the nonlinear material response.[1,2,16] However, when the confinement is provided by the sharp, thresholdlike response of the material to the light energy deposition, the role of fluctuations just near the threshold level are of great importance. We do not discuss the fluctuations within the laser beam[15] but the fluctuations of the material response when the laser intensity distribution is carefully controlled.

In the present paper, we study the confinement conditions when the threshold is provided by the percolation transition.[17] Percolation denotes establishing long-range connectivity in random media. The simplest models are site and bond percolation on a lattice. For site percolation on the lattice, each site of the lattice is considered to be either occupied or not occupied. The occupation is random with some probability p. The adjacent occupied sites are assumed to be "connected" to one another. In this way, the formation of vast connectivity clusters can occur. For bond percolation, bonds between neighboring sites either exist or not exist randomly

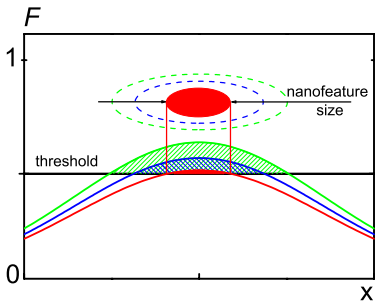

FIG. 1. (Color online) Scheme of the laser modification of a threshold material. The curves represent the distributions of the deposited laser energy density over a coordinate. Formation of the nanofeature is expected only where the threshold is exceeded. Reduction in the feature size is achieved by performing the modification in the regime when the magnitude of the distribution of the deposited energy is kept close to the threshold.

with some probability, p, and the connectivity is established through the bonds.

Percolation is an example of a connectivity phase transition.[17,18] In the thermodynamic limit, i.e., when the lattice dimensions are infinite, the increase in the occupation probability, p, above the threshold value results in the formation of an infinite cluster. For such a transition, the average density of the infinite cluster, P_{inf}, is considered to be the order parameter. The order parameter continuously increases only when $p > p_{th}$ whereas if $p < p_{th}$, P_{inf} equals zero. Near the threshold, the order parameter is known to obey the following scaling law:

$$P_{\text{inf}} \propto (p - p_{th})^{\beta}. \tag{1}$$

The correlation length that determines the size of the nonhomogeneities inside the infinite cluster is given by another scaling relation,

$$\xi \propto |p - p_{th}|^{-\nu}. \tag{2}$$

The values of scaling exponents, $\nu \approx 0.88$ and $\beta \approx 0.41$, are fixed within the universality class of three-dimensional percolation.[17]

The setting of the problem of confined percolation is imposed by the growing development of the two-photon polymerization (TPP) technique. This technique is a leading technology for creating complex structures in three dimensions with submicron resolution.[19–22] The photons absorbed within the polymerizable medium (resin or resist) trigger the set of chemical reactions that involve the monomer, the main component of the resin or resist. The reacted monomer molecules attach to each other and, consequently, form branchy macromolecules. When the fraction of the reacted monomer molecules, the conversion, becomes high enough, the connectivity phase transition occurs. Such a transition denotes the appearance of the macroscopically sized network of interconnected monomer molecules (the gel). This gel acts as a mechanically and chemically stable framework for the resulting polymer. After irradiation, the samples are developed in the dissolver and dried. Only the domains where the macroscopic network exists can survive this postprocessing stage and form the resulting polymer feature.

The polymer network is a result of many chemical reactions, including the growth of polymer chains, the crosslinking of chains, and others. Each separate reaction act occurs stochastically thus resulting in randomness of the polymer network. In specific polymerizing systems, the randomness can also be affected by local variations in reaction kinetics thus resulting in some microheterogeneity.[23] However, both polymerization and percolation exhibit the connectivity threshold and similar near-threshold scaling laws. Therefore, the polymerization process is often modeled by means of percolation.[18,24] Within the model, the local conversion (i.e., the fraction of the reacted monomers) corresponds to the site or bond occupation probability, p. The macromolecules are modeled by the clusters, among which the ones of macroscopic size represent the polymer features. Such a model corresponds to the case, when all the monomers are of the same type (homopolymerization) and are able to crosslink (multifunctional monomer).

Thus, the problem of the spatial confinement of percolation is closely related to the problem of the spatial resolution of nanomodification. However, the phase transitions are sharp only when an infinite sample is considered, i.e., in the thermodynamical limit. At a nanoscale, the finite-sized phenomena can become significant. Thus, even if the modification threshold is overcome within some domain of the sample, as shown in Fig. 1, the actual nanofeature may be missing due to a fluctuation or it may occur at an unpredictable location. These phenomena may limit the applications of the laser nanostructuring.

In this paper, the minimal size of a spherical nanofeature that remains stable against fluctuations is addressed. We perform Monte Carlo modeling of the percolation with the spherically symmetrical occupation probability distribution that is constrained in three dimensions. The actual nanofeature is represented by the largest interconnected cluster. By analyzing the ensembles of such clusters, we find two different statistical regimes. In the former case, within the nanofeature, one can select the domain that is stable against the fluctuations, i.e., the kernel. In the latter case, such a domain is absent. These two regimes are clearly demarcated by the critical size. We propose an analytical model to obtain the formula for such a limiting size.

II. NUMERICAL EXPERIMENT

In this section, we model the site percolation on the cubic lattice with the Monte Carlo technique and examine the case when the site occupation probability is not uniform over the lattice but is given by a smooth, three-dimensionally constrained distribution, $p(\vec{r})$. In this numerical experiment, the largest connected cluster of occupied sites is examined for different parameters of the distribution. We analyze the possibility that the largest cluster is localized within the boundaries set by the percolation threshold, p_{th} (see Fig. 1).

For simplicity, the spherically symmetric Gaussian distribution profile is chosen,

$$p(\vec{r}) = A \exp(-r^2/2w^2). \tag{3}$$

The radius of the domain where the percolation threshold is exceeded is then obtained from Eq. (3),

$$r_{th} = w\sqrt{2 \ln(A/p_{th})}.$$

This radius may be changed both by varying the magnitude, A, with respect to the threshold level, as shown in Fig. 1, and by changing w. In most of the numerical experiments described below, the magnitude is kept fixed while the width of the distribution is varied.

The percolation is a connectivity phase transition. The order parameter for such a transition is the average density of the infinite cluster. Thus, we have initially modeled the spatial distributions, $P(r)$, of the local ensemble-average density of the largest cluster. The density of the largest cluster at point $\vec{r}$ is calculated as $P(\vec{r}) = N_{occcupied}(\vec{r})/N_{total}$, where N_{total} is the total number of implementations in the ensemble and $N_{occcupied}(\vec{r})$ is the number of implementations in which the site situated at $\vec{r}$ belongs to the largest cluster. In Fig. 2, the

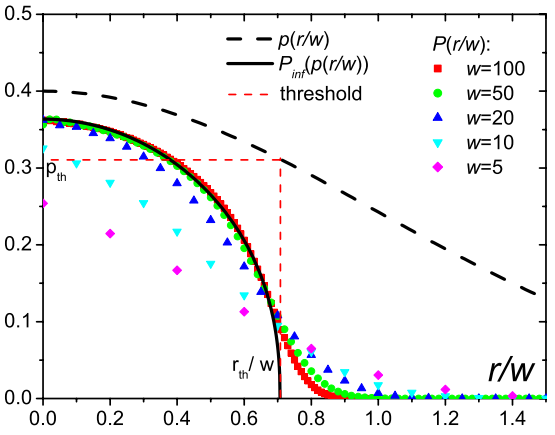

FIG. 2. (Color online) Results of the modeling of site percolation with the Gaussian spherically symmetrical spatial distribution of occupied sites. Probability $p(r/w)$ that a site is occupied at a given reduced radius is plotted with the dashed line (w is the width of the Gaussian distribution measured in the lattice periods). Scatter plots represent the density distributions of the largest cluster for different values of w. The limiting case, $w\to\infty$, is indicated by a solid line. The latter graph is obtained by considering the density of the infinite cluster in the ordinary percolation problem with the occupation probability level corresponding to the local value of $p(r/w)$. The dashed line also emphasizes the percolation threshold.

distributions of the density of the largest cluster (averaged over 10 240 implementations) are plotted for different Gaussian widths, w, and a fixed Gaussian magnitude of $A=0.4$ (the percolation threshold is[17] $p_{th}\approx 0.3116$). The occupation probability distribution, $p(r)$, is also included in the graph. The corresponding values of the percolation order parameter, $P_{\text{inf}}[p(r)]$, are indicated for comparison. The percolation order parameter corresponds to the limit of P at $w\to\infty$.

For $w=100$ and $w=50$ lattice periods, there is a zone near the center where $P\approx P_{\text{inf}}$. This zone, which is referred to as the kernel, is not affected by the spatial constraints of the distribution, $p(r)$. Outside of this zone, the average local density depends on w. As seen in Fig. 2, for the narrower probability profiles with widths of 10 and 5 lattice periods, the kernel disappears.

Furthermore, we investigate how the average statistical parameters of the largest cluster depend on the width, w of the occupation probability distribution while keeping its magnitude, A, fixed. Among the statistical parameters of the largest cluster is the average mass as well as the dispersions of the size and the position.

The mass, M, indicates the number of sites that belong to the largest cluster. The position of the cluster is given by its center of mass, $\vec{r}_{cmass}=M^{-1}\Sigma_i\vec{r}_i$, where $\vec{r}_i$ represents the radius vectors for all of the sites within the cluster. The size of the cluster is determined by its gyration radius, $r_{gyr}=\sqrt{M^{-1}\Sigma_i(\vec{r}_i-\vec{r}_{cmass})^2}$. The dispersions $D[\vec{r}_{cmass}]$ and $D[r_{gyr}]$ over several implementations indicate the strength of the fluctuations of the position and the size of the cluster, respectively. The dispersions are understood as $D[a]=\langle(a-\langle a\rangle)^2\rangle$, where $\langle\ \rangle$ represents the ensemble average. The ratio of the average masses of the two largest clusters, $g=\langle M_2\rangle/\langle M\rangle$, indicates the degree of fragmentation within the large clusters.

For the largest cluster, we plot the dispersion of the coordinate (z, for certainty) of the center of mass ($D[z_{cmass}]$), the dispersion of the gyration radius ($D[r_{gyr}]$), the degree of fragmentation (g), and the average mass ($\langle M\rangle$) against the Gaussian width, w. In Figs. 3(a) and 3(b), those plots are generated for $A=0.38$ and $A=0.34$, respectively. The ensemble averages are taken over 10 240 implementations.

In each of the two sets of graphs, a single pronounced spatial scale is clearly evident. For certainty, we fix this critical scale, w_{cr}, with the position of the maximum of $D[z_{cmass}]$. At $w>w_{cr}$, the mass of the largest cluster approaches the scaling law $M\propto w^3$ whereas at $w<w_{cr}$, the scaling exponent becomes less than 3. This can be explained by the appearance of the kernel when w exceeds w_{cr}. The mass of the cluster can be obtained by the integration of the cluster density, P, over space. Within the kernel, the local average density depends only on the occupation probability, i.e., $P(r)=P[p(r/w)]$. If the cluster almost entirely consists of the kernel (as seen in Fig. 2, for $w=100$), then

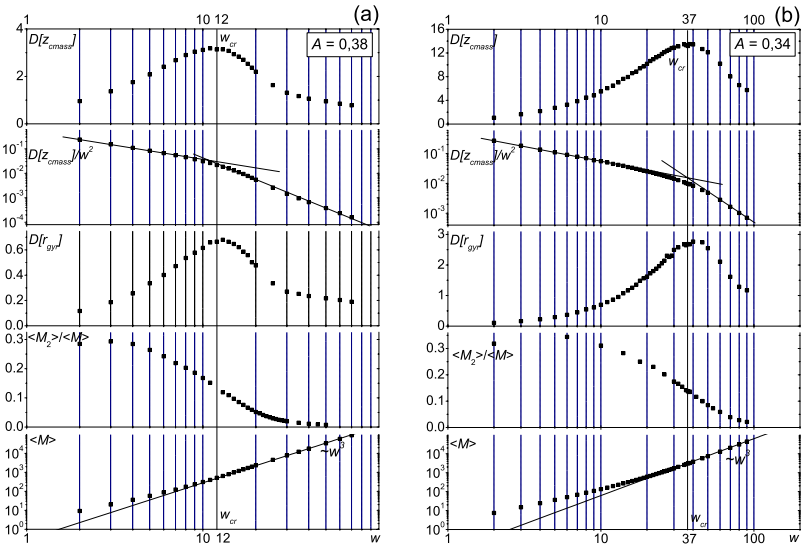

FIG. 3. (Color online) Average parameters of the largest cluster obtained with the Gaussian-distributed occupation probability. The parameters include (from top to bottom) the dispersion of a coordinate of the center of mass of the cluster; the same dispersion but normalized by the square of the distribution width; the dispersion of the gyration radius of the cluster; the ratio of the average masses of two largest clusters; and the average mass of the largest cluster. The plots represent the dependencies of the parameters on the width, w, of the Gaussian distribution of the occupied sites while keeping its magnitude, (a) $A=0.38$ and (b) $A=0.34$, fixed.

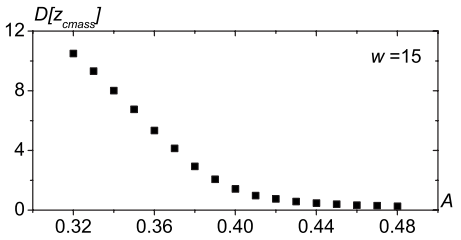

FIG. 4. Percolation with the Gaussian distribution of the occupied sites. Dispersion of a coordinate of the center of mass of the largest cluster for different magnitudes of the Gaussian and a fixed width of $w=15$ lattice periods.

$$M = \int_{R^3} P(r)d^3\vec{r} \approx w^3 \int_{R^3} P[p(r/w)]d^3(\vec{r}/w) \propto w^3.$$

As seen in the graphs, the decrease in w below the critical scale leads to a dramatic increase in the fragmentation of the large clusters. Both $D[z_{cmass}]$ and $D[r_{gyr}]$ have maxima at $w \approx w_{cr}$. The decrease in the dispersions for a narrow $p(r)$ (i.e., when $w < w_{cr}$) can be explained by the spatial constraints imposed on the cluster by the distribution of the occupation probability itself. At $w > w_{cr}$, the presence of the kernel decreases the fluctuations within the cluster, thereby again reducing the dispersions. To eliminate the effect of the spatial constraints at $w < w_{cr}$, we plot the normalized dispersion, $D[z_{cmass}]/w^2$. The normalized dispersion is a monotonous function that fits the power laws well, both at $w < w_{cr}$ and $w > w_{cr}$. Near the critical width, the exponent of the power law changes, indicating the demarcation between the two regimes. When exceeding w_{cr}, the fluctuation strength decreases steeply.

A comparison between Figs. 3(a) and 3(b) shows that the critical width, w_{cr}, depends on the magnitude of the occupation probability profile, A. This is also evident in Fig. 4, where $D[z_{cmass}]$ is plotted against A while w is kept fixed. The fluctuations of the position of the largest cluster start growing only when A decreases below $A_{cr} \approx 0.4$.

The typical implementations of the largest cluster formed in both regimes are presented in Figs. 5(a) and 5(b). As evident in Fig. 5(a), the main part of the largest cluster with the kernel reliably fits the expectation given by the percolation threshold. Thus, such a nanofeature can serve as the simplest "brick" for the formation of complex structures. Without the kernel [Fig. 5(b)], the cluster is not localized within the bounds given by the percolation threshold. Instead, it is randomly positioned within and near the domain where the threshold is exceeded.

In this section, it has been exhibited that the largest cluster of the occupied sites distributed by the Gaussian over the cubic lattice can be formed in two different statistical regimes. The regimes are demarcated by the critical width, w_{cr}, of the occupation probability distribution. When $w > w_{cr}$, the implementations of the cluster are almost entirely localized within the bounds given by the percolation threshold. When the distribution becomes narrower than w_{cr}, the fluctuations of the size and position of the cluster drastically increase and the localization vanishes. The critical width, w_{cr}, depends on the magnitude of the Gaussian probability profile. In the next section, we obtain this dependence analytically within the framework of the gradient percolation theory.

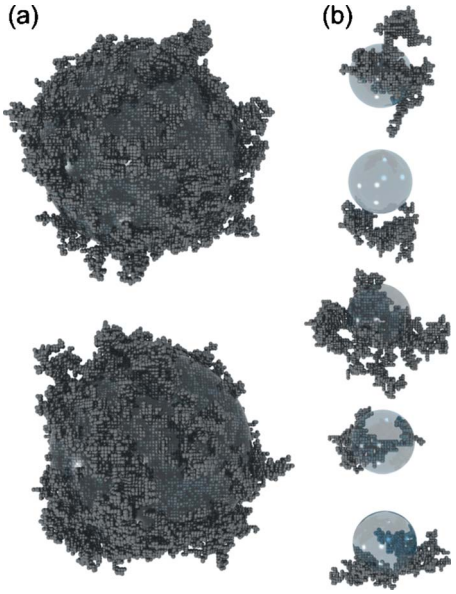

FIG. 5. (Color online) Typical implementations of the largest cluster (a) comprising and (b) not comprising the kernel. The cluster is formed by the percolation of the occupied sites distributed by the Gaussian. The "metallic" spheres represent the occupied sites that belong to the largest cluster. The threshold level is indicated by the "glass" sphere.

III. GRADIENT PERCOLATION MODEL

The gradient percolation model[25] is used when the occupation probability has a nonuniform spatial distribution, i.e., when $p(\vec{r}) \neq \text{const}$. Such a model was previously employed to investigate different phenomena, including the propagation of diffusion fronts[25–28] and the corrosion and etching of materials.[29–31]

The gradient percolation has been studied previously[25–31] for the case of the monotonous change in the occupation probability along a single Cartesian coordinate (x). In that case, the cluster that is finite over x and infinite over the other dimension(s) can be obtained. The average depth, x_{th}, to which the infinite cluster penetrates along the x dimension is determined by the percolation threshold, $p(x_{th})=p_{th}$. For the linear dependence of

$$p(x) = 1 - x/L, \tag{4}$$

the fluctuations of the cluster depth are found to reside within a layer of thickness,

$$\sigma_h \propto L^{\nu/1+\nu}. \tag{5}$$

Here, ν is the exponent of the scaling relation (2) that determines the typical size of the nonhomogeneities inside the infinite cluster in the ordinary (nongradient) percolation problem. Outside the fluctuation zone, i.e., far from the boundary, the density, P, of the infinite cluster proves to be the same as the one obtained for the ordinary percolation, i.e., $P \approx P_{\text{inf}}[p(x)]$.

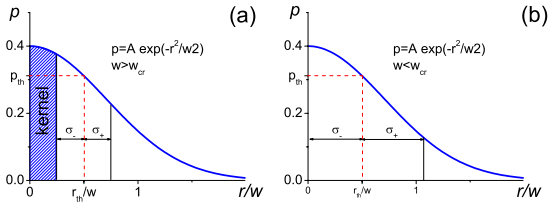

FIG. 6. (Color online) Kernel and layer of fluctuations. Gaussian site occupation distributions of a width (a) greater than critical and (b) smaller than critical are plotted with a diagonal line. The dashed line indicates the threshold level.

In the above section, we consider the spherically symmetrical distribution of $p(r)$. The results of the numerical experiment (see Fig. 2) can be interpreted in terms of the existence of the fluctuation layer at $r \in [r_{th}-\sigma_-, r_{th}+\sigma_+]$.

The largest cluster is formed either with or without the kernel, depending on whether $\sigma_- < r_{th}$ (see Fig. 6). If $\sigma_- < r_{th}$, the kernel is formed at $r \in [0, r_{th}-\sigma_-)$. Otherwise, only the fluctuation zone exists. The demarcation between the two regimes is given by $r_{th}=\sigma_-$. Hence, a proper definition of σ_- is required to determine the critical parameters of the site occupation probability distribution. For that, in the present paper, we propose an approach based on the correlation length.

First, we consider the planar geometry of the occupation probability distribution: $p=p(x)$. For the ordinary spatially uniform percolation problem, the correlation length, ξ [see Eq. (2)], determines the typical size of the stochastic nonhomogeneities within the infinite cluster. This is actually the scale of decay of the correlation function of the fluctuations within the infinite cluster. In our phenomenological model, we treat ξ similarly to the light penetration depth in the absorbing media. Then, $1/\xi$ plays the role of the "extinction" coefficient for the fluctuations. For the nonhomogeneous layered media, we introduce the decay integral,

$$\int_{x_0}^{x_1} \frac{dx}{\xi[p(x)]} \tag{6}$$

which is expected to determine the correlation decay over the thick layer with a distribution, $p(x)$, of the occupation probability.

Next, we consider the fluctuation layers $x_{th}-\sigma_- < x < x_{th}$ and $x_{th} < x < x_{th}+\sigma_+$ near the threshold point, x_{th}. In our model, the thicknesses, σ_- and σ_+, are governed by the level of the correlation decay from the threshold position towards the boundaries of the fluctuation zone. This level is determined by the phenomenological value of the decay integral. Near the threshold position, the scaling law [Eq. (2)] is fulfilled. Thus, the decay integrals over the fluctuation zone can be written as

$$b = \int_{x_{th}-\sigma_-}^{x_{th}} |p(x) - p_{th}|^{\nu} dx \tag{7a}$$

and

$$b = \int_{x_{th}}^{x_{th}+\sigma_+} |p(x) - p_{th}|^{\nu} dx. \tag{7b}$$

The phenomenological parameter b depends on the type of percolation problem (bond or site percolation, lattice type or the formulation of the continual percolation problem) but it does not depend on the distribution of p.

By means of Eqs. (7a) and (7b), both σ_- and σ_+ can be obtained. These formulae can be treated as a reformulation of the estimation $\sigma_h \propto \xi[p(x_{th} \pm \sigma_h)]$, which can be found, for instance, in Ref. 32.

For the linear distribution [Eq. (4)] of the occupation probability p, the resulting thicknesses of the fluctuation layer are calculated using formulae (7a) and (7b),

$$\sigma_{\pm} = [(1+\nu)b]^{1/1+\nu} L^{\nu/1+\nu}. \tag{8}$$

This result repeats the scaling law [Eq. (5)] mentioned above.

Employing the above approach, one can construct a similar model for a spherically symmetrical distribution of the occupation probability, $p(r)$. We assume that $p(r)$ increases towards the center, reaching the threshold level at r_{th}, which is obtained from the equation $p(r_{th})=p_{th}$. Similar to the one-dimensional problem, the largest cluster is expected to reside at $r \in [0, r_{th}+\sigma_+]$. Near the threshold radius, r_{th}, there is a zone of fluctuations at $r \in [r_{th}-\sigma_-, r_{th}+\sigma_+]$ (see Fig. 6). The kernel is formed in the center of the cluster if $r_{th} > \sigma_-$. Otherwise, the nanofeature possesses only the fluctuation zone.

The primary goal of our model is to determine the parameters of the probability distribution, $p(r)$, that leads to the presence of the kernel in the largest cluster. The boundary case between the cluster with and without the kernel is given by the relation $r_{th}=\sigma_-=r_{cr}$. We denote r_{cr} as the critical value for the threshold radius that corresponds to this boundary case.

The value of σ_- is obtained from Eq. (7a),

$$b = \int_0^{r_{cr}} |p(r) - p_{th}|^{\nu} dr. \tag{9}$$

To produce a simple formula for r_{cr}, we expand $p(r)$ in a series near $r=0$ and then take the first two nonzero expansion members,

$$p(r) = A - \frac{A - p_{th}}{r_{th}^n} r^n + \cdots. \tag{10}$$

The relation $p(r_{th})=p_{th}$ is taken into account. The substitution of $p(r)$ in Eq. (9) by the above expansion results in

$$b = (A - p_{th})^{\nu} \int_0^{r_{cr}} \left| 1 - \frac{r^n}{r_{cr}^n} \right|^{\nu} dr = (A - p_{th})^{\nu} r_{cr} K_n, \tag{11}$$

where $K_n = n^{-1} B(n^{-1}, \nu+1)$ and $B(\,)$ is the Euler beta function. The exponent $\nu \approx 0.88$ is within the universality class of three-dimensional percolation problems. Thus, $K_1=(1+\nu)^{-1} \approx 0.53$, $K_2 \approx 0.69$, $K_3 \approx 0.77$, etc. By rearranging the above expression, we obtain the final formula for the critical threshold radius,

$$r_{cr} = \frac{bK_n^{-1}}{(A - p_{th})^{\nu}}. \tag{12}$$

With this formula, one can obtain the critical size of the occupation probability distribution for a fixed magnitude. It can be easily rewritten to obtain the critical magnitude, A_{cr}, for a given threshold radius, r_{th},

$$A_{cr} - p_{th} = \left(\frac{b}{K_n}\right)^{1/\nu} r_{th}^{-1/\nu}. \tag{12'}$$

Equations (12) and (12′) are based on approximation (10) for the occupation probability distribution. In some cases (flat-top distribution, for instance), such an approximation fails and the critical radius must be obtained directly from Eq. (9) by considering the correlation integral.

Equation (12′) is consistent with the finite-size scaling concept.[17] In the case of the occupation probability being constant, the percolation threshold, p_L, for a finite lattice deviates from the threshold, p_{th}, for the infinite lattice. The scaling law for this deviation is

$$p_L - p_{th} \propto L^{-1/\nu}, \tag{13}$$

where L is the size of the lattice. Thus, A_{cr} can be understood as an effective percolation threshold that must be exceeded to form the cluster with the kernel. The extra occupation probability needed to form the kernel corresponds to the size of the distribution according to the finite-size scaling law [Eq. (13)].

For the Gaussian distribution [Eq. (3)], one can calculate the critical width of the profile instead of the critical threshold radius,

$$w_{cr} = \frac{K_2^{-1} b}{(A - p_{th})^{\nu}\sqrt{2\ln(A/p_{th})}}. \tag{14}$$

Now, one can directly compare the calculated critical width with the width obtained by means of Monte Carlo modeling. In Fig. 7, a comparison is presented for both bond and site percolation on a cubic lattice. Additionally, the percolation of short "polymer chains" has been modeled. In the latter case, each site of the lattice has a probability of $p(r)$ to start a random walk of 20 connected bonds, i.e., the chain. These chains form clusters by intersecting with each other similar to ordinary bond percolation. This chain model is closer to the polymerization problem discussed later.

It is noticeable that the results obtained with all three models fit the analytical formula obtained above well. Significant deviation is only observed in the last model when attempting to make the distribution of the probability narrower than the size of a single 20-bond chain. Indeed, in Fig. 7, for the point emphasized by a dashed circle, the width of the Gaussian is $w=4$ lattice periods whereas the size of a chain of 20 bonds is approximately[24] $20^{1/2} \approx 4.47$. In this case, the fluctuations within the single chain become important; however, such fluctuations are not considered in our model.

The only parameter that has been tuned to fit the curves is b (except the percolation of the chains, where p_{th} is also unknown). The parameter b indicates the integral reduction

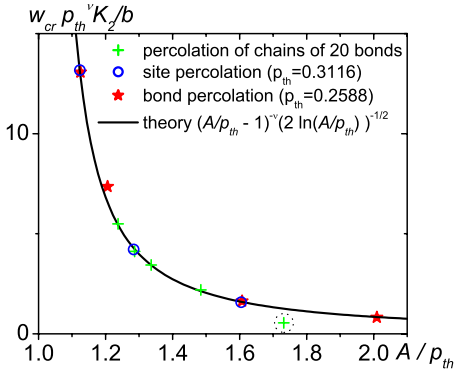

FIG. 7. (Color online) Comparison of the analytical model with the Monte Carlo simulations of the percolation with the Gaussian spatial distribution of the occupation probability, $p(r)$. In all of the graphs, the normalized critical width of the Gaussian is plotted against its normalized magnitude. The simulation was performed for site percolation (circles), bond percolation (stars), and the correlated percolation of the 20-bond chains that initiate in a site of the lattice with probability $p(r)$. The analytical calculation is indicated by a solid line. The only point at which a significant deviation from the model is observed is emphasized with a dashed circle. The percolation thresholds for site and bond percolation on the cubic lattice are taken from Ref. 17. To fit the model with the theory, the parameter values of $b=0.47$ for site percolation, $b=0.25$ for bond percolation, and $b=0.30$ and $p_{th}=0.040$ for the percolation of chains have been employed; $\nu=0.88$ and $K_2=0.69$.

in the correlation function within the fluctuation zone. According to our model, it does not depend on the shape of the probability profile. Here, we check this by modeling the distribution p that is substantially different from the Gaussian. For example, the "conelike" distribution,

$$p(\vec{r}) = \begin{cases} A\dfrac{w - r}{w}, & r < w \\ 0, & r \geq w \end{cases} \tag{15}$$

has a nonzero derivative dp/dr at the center and thus is expanded in a series in Eq. (10) differently from the Gaussian. Thus, one can expect that for the conelike distribution, the critical radius is given by Eq. (12) with coefficient K_1 instead of K_2 but with the same parameter b. We check this in Fig. 8, where the critical radius obtained from the analytical model is compared to the one from the Monte Carlo numerical experiment. For both for the Gaussian and the conelike distributions, the same fitting value of $b \approx 0.47$ has been obtained for site percolation on the cubic lattice.

The statistically stable largest cluster includes both the kernel and the fluctuation zone. The fluctuation zone is the layer that has a thickness of σ_- from the threshold radius toward the center and a thickness of σ_+ toward the outside. In this paper, σ_- has been examined carefully, and the relation of σ_- to the critical width has been proven. By employing σ_+ calculated in the same way as σ_- with formula (7b), we estimate the total size of the largest cluster to be $r_{total}=r_{th}+\sigma_+$. This value is always larger than r_{th}, which is predicted by the percolation threshold. To evaluate σ_+, $p(r)$ is linearized near $r=r_{th}$,

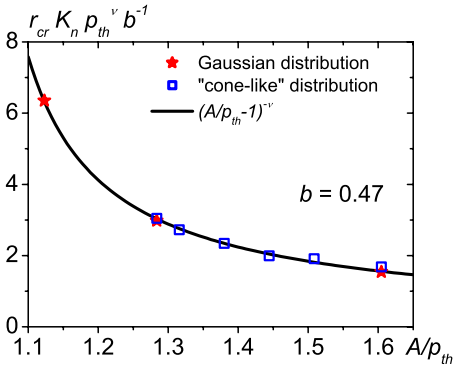

FIG. 8. (Color online) (Color online). Results of Monte Carlo simulations of site percolation with different distributions of the occupation probability. The Gaussian (stars) and conelike (squares) distributions are considered. In all of the graphs, the normalized critical radius is plotted against the normalized magnitude of the distribution, and $\nu=0.88$ and $p_{th}=0.3116$. For the Gaussian distribution $K_n=K_2=B(1/2,\nu+1)/2\approx 0.69$, and for the conelike distribution, $K_n=K_1=(1+\nu)^{-1}\approx 0.53$. Comparison with the analytical model (solid line) is performed. According to the analytical model, the phenomenological parameter b must be the same for both of the distributions. Indeed, with $b=0.47$, the datasets for both probability profiles fit the analytical curve well.

$$p(r) = p_{th} + \frac{dp(r_{th})}{dr}(r - r_{th}). \tag{16}$$

Then, from Eq. (8),

$$\sigma_+ \approx [(1+\nu)b]^{1/1+\nu} \left| \frac{dp(r_{th})}{dr} \right|^{-\nu/1+\nu}, \tag{17}$$

where $1/L$ from the original expression is substituted by the derivative.

When the width of the probability profile is far above the critical one, w_{cr}, both σ_+ and σ_- are obtained from the linearized expression (17). Hence,

$$\sigma_+ + \sigma_- \propto w^{\nu/1+\nu}. \tag{18}$$

Because $r_{th} \propto w$ and $\nu/(1+\nu)<1$, the thickness of the fluctuation layer grows slower than the overall size of the cluster. In the three-dimensional case, $\nu\approx 0.88$ and $\sigma_{\pm} \propto w^{0.45}$. This indicates that for the clusters, which are much larger than the critical size, the fluctuation zone can be neglected.

IV. APPLICATIONS FOR TWO-PHOTON POLYMERIZATION

In this section, we discuss the application of the theoretical results obtained above to TPP. TPP (Refs. 19–22) is a laser three-dimensional lithography technique that is capable of producing polymer structures with 100 nm spatial resolution. The structures are obtained through direct writing with the focused laser beam in the sample of the polymerizable resist or resin. The physicochemical process that is behind this technology is photopolymerization. The absorption of the laser light by the photoinitiator molecules within the polymerizable medium causes their decomposition into active species (free radicals, ions, etc.). Each of the active species can attach many molecules of the monomer, which is the main component of the polymerizable composition, resulting in the formation of the polymer chain. Due to the crosslinking reactions, the distinct chains become connected to each other, assembling into polymer networks. The crosslinking polymerization involves the connectivity phase transition that is similar to the percolation. The establishment of connectivity indicates the formation of the macroscopically sized network of polymer chains (the gel) during the polymerization process. The appearance of the gel is associated with the certain level of the conversion, i.e., the fraction of the monomer molecules that are included in the polymer chains. Near the threshold point, the scaling relation (2) is also fulfilled. This allows us to employ the same phenomenological model for confinement in photopolymerization as the one proposed above for confinement in percolation.

The final distribution of the conversion, $p(\vec{r})$, is formed as a result of irradiation by the laser with the intensity distribution $I(\vec{r},t)$. The interrelation between the conversion and laser intensity can be rather complex. The photochemistry of the polymerization, the change in the refractive index during the process,[33] the diffusion of the reacting species,[34] and other phenomena must be considered. However, making a proper model of laser polymerization is beyond the scope of this work. Here, we show only an example of how the proposed model of spatial confinement can be reformulated in terms of the laser field parameters for the case of TPP.

In this paper, we assume the two-photon absorption mechanism. However, for the laser nanopolymerization, the actual light absorbtion and photoinitiation mechanisms are being discussed.[35,36] For the two-photon absorption, the energy density, F, absorbed during N pulses of length τ_{pulse} is proportional to the square of the laser intensity, I,

$$F(\vec{r}) = N\beta \int_0^{\tau_{pulse}} I^2(\vec{r},t)dt, \tag{19}$$

where β is the two-photon absorption coefficient. Let us consider the formation of a nanofeature with a single femtosecond pulse (or a series of pulses) that is short as compared to the time scales of the modification. Additionally, we neglect the nonlocal phenomena, such as the diffusion of reacting species. In such a case, the total number of reacted monomer molecules within a domain of the polymerizable medium depends only on the number of photons absorbed in this domain. This simple zero-dimensional model leads to the local dependence of the conversion on the absorbed energy density in the form of a function, $p=p[F(\vec{r})]$. One can define the threshold energy density, F_{th}, that is needed to reach the threshold conversion level.

Then, near the threshold,

$$p \approx p_{th} + \frac{dp(F_{th})}{dF}(F - F_{th}). \tag{20}$$

Using Eq. (20), one can rewrite the scaling law [Eq. (2)] as

$$\xi = \xi_0 \left[\frac{dp(F_{th})}{dF} \right]^{\nu} (F - F_{th})^{\nu}. \tag{21}$$

Using Eq. (21) instead of Eq. (2), one can derive the formulae for r_{cr} and σ_+ in the same manner as described for Eqs. (12) and (17),

$$r_{cr} = K_n^{-1} L_{mat} \left(\frac{F_{\max}}{F_{th}} - 1 \right)^{-\nu} \tag{22}$$

and

$$\sigma_+ = [(1+\nu)L_{mat}]^{1/1+\nu} \left| \frac{d}{dr} \left[\frac{F(r_{th})}{F_{th}} \right] \right|^{-\nu/1+\nu}. \tag{23}$$

The length,

$$L_{mat} = b \left[F_{th} \frac{dp(F_{th})}{dF} \right]^{-\nu} \tag{24}$$

depends on the material being processed by the laser. L_{mat} is the only parameter in formulae (22) and (23) because the exponent ν is fixed within the universality class. Thus, all of the necessary photophysical properties of the material are now compacted into a single phenomenological parameter, L_{mat}.

The derivation of formulae (22)–(24) is based on an assumption of the local response of the material to the absorbed laser radiation. However, in many cases, one must consider the nonlocal phenomena along with the fluctuations. For instance, the diffusion of free radicals during TPP was proven to be important.[34] Shrinkage of the polymer during postprocessing may cause significant distortions in the size and shape of the final observed structures.[37]

One of the most important issues in TPP is the minimal size of the simplest nanofeature, the voxel, which determines the miniaturization capabilities of TPP. From the perspective of fluctuations, this issue can be addressed using the model above. We can consider again formulae (12) and (17). The spatial distribution of the conversion, $p(r)$, is expanded in a Taylor series, and the first two nonzero members are taken,

$$p = A + \frac{1}{2} p''(0) r^2. \tag{25}$$

The minimal feature size is obtained when the critical parameters of the conversion distribution are taken. Thus,

$$p_{th} = A + \frac{1}{2} p''(0) r_{cr}^2. \tag{26}$$

From Eqs. (12) and (26), one derives

$$r_{cr} = \left(\frac{b}{K_2} \right)^{1/1+2\nu} \left[\frac{|p''(0)|}{2} \right]^{-\nu/1+2\nu} \tag{27}$$

and from Eqs. (17) and (26), one obtains

$$\sigma_+ = \left[\frac{(1+\nu)K_n}{2^{\nu}} \right]^{1/1+\nu} \cdot r_{cr}. \tag{28}$$

Finally,

$$r_{total} = r_{cr} + \sigma_+ \propto |p''(0)|^{-\nu/1+2\nu}. \tag{29}$$

We find that the minimal size of the nanofeature is determined by the second derivative of the probability distribution at the point of maximum. Regardless of the fact that TPP has a modification threshold, the sharper the conversion distribution, the smaller is the size of the voxels that can be potentially obtained. The sharper conversion distribution can be obtained both by controlling the distribution of the incident laser field and by choosing the appropriate components of the polymerizable medium and their proportions. In the latter case, the nonlocal and nonlinear phenomena during the photopolymerization process on the nanoscale must be studied and utilized.

V. DISCUSSION AND CONCLUSIONS

We expect the above model to be valid for different types of critical phenomena that obey the scaling laws similar to Eq. (2). In particular, for the thermal phase transitions of the second kind, the correlation length is known to obey the scaling relation,

$$\xi = \xi_0 \left| \frac{T - T_{th}}{T_{th}} \right|^{-\nu} \tag{30}$$

near the transition point.[38] T is the temperature and T_{th} is the transition temperature. We expect that for the thermal transitions of the second kind, formulae (12) and (17) are also valid with p, p_{th}, and A substituted by T/T_{th}, 1, and $T_{\max}/T_{th}$, respectively (here, $T_{\max}$ is the maximum temperature in the distribution).

The resulting expressions are

$$r_{cr} = \frac{bK_n^{-1}}{(T_{\max}/T_{th} - 1)^{\nu}}, \tag{31}$$

$$\sigma_+ = ((1+\nu)b)^{1/1+\nu} \left| \frac{1}{T_{th}} \frac{dT(r_{th})}{dr} \right|^{-\nu/1+\nu}. \tag{32}$$

In summary, we perform the Monte Carlo modeling of the spatial confinement of percolation. We model the site percolation on a cubic lattice and examine the case when the site occupation probability is not uniform over the lattice but is given by a smooth three-dimensionally constrained distribution (p distribution) characterized by its magnitude and width. In this numerical experiment, we study the structure of the largest interconnected cluster obtained when the p-distribution magnitude slightly exceeds the percolation threshold. The distribution is varied by changing either the width or the magnitude while keeping another parameter fixed.

According to the results of our numerical experiment, the largest cluster possesses the fluctuation zone and the kernel, which is the domain that is stable against fluctuations. When varying the width of the p distribution at a fixed magnitude, one receives either the cluster with or without the kernel. These two regimes are clearly demarcated by the critical width of the p distribution.

The implementations of the largest cluster without the kernel drastically differ from each other, exhibiting significant distortions and even splitting into pieces. The kernel

provides stability to the structure of the cluster.

We present the analytical model that relates the magnitude of the p distribution with its critical width. This formula also allows for estimation of the radius of the kernel and the size of the fluctuation zone within the cluster. This model is shown to match with the numerical experimental data.

The problem of the spatial confinement of percolation is closely related to the problem of the spatial resolution of nanopolymerization. The connectivity transition that is similar to percolation provides a sharp, thresholdlike response of the polymerizable media to the laser exposure. The results of this paper show that if the processing of the material by the laser beam is performed too close to the threshold level, instead of obtaining the nanofeature with an arbitrarily small size overcoming the diffraction limit, one faces distortions in the formed structures governed by fluctuations. The presence of the kernel does not guarantee the small size of the voxel. Even if the laser power is increased to obtain the voxel with the kernel, the surrounding soft part of the voxel is inevitably formed. This imposes natural limitations on the spatial resolution of nanopolymerization. Here, we consider the fluctuations of the material response but not the fluctuations of the laser beam.

ACKNOWLEDGMENTS

This paper was financially supported in part by the RFBR under Grant No. 09-02-00665-a and by the Program of presidium of the Russian Academy of Sciences "Extreme light fields and applications."

*bit@appl.sci-nnov.ru

[1] D. Bäuerle, *Laser Processing and Chemistry*, 3rd rev. ed. (Springer, Berlin, 2000).
[2] N. Bityurin, Annu. Rep. Prog. Chem., Sect. C: Phys. Chem. **101**, 216 (2005).
[3] H. Fukumura, N. Mibuka, S. Eura, and H. Masuhara, Appl. Phys. A **53**, 255 (1991).
[4] F. Beinhorn, J. Ihlemann, K. Luther, and J. Troe, Appl. Phys. A **68**, 709 (1999).
[5] A. Yu. Malyshev, N. A. Agareva, O. A. Mal'shakova, and N. M. Bityurin, J. Opt. Technol. **74**, 641 (2007).
[6] N. Bityurin, Appl. Surf. Sci. **255**, 9851 (2009).
[7] E. Mcleod and C. B. Arnold, Nat. Nanotechnol. **3**, 413 (2008).
[8] T. C. Chong, M. H. Hong, and L. P. Shi, Laser Photonics Rev. **4**, 123 (2010).
[9] A. I. Kuznetsov, J. Koch, and B. N. Chichkov, Appl. Phys. A **94**, 221 (2009).
[10] D. Parthenopoulos and P. Rentzepis, J. Appl. Phys. **68**, 5814 (1990).
[11] S. Kawata and Y. Kawata, Chem. Rev. **100**, 1777 (2000).
[12] N. Bityurin, B. S. Luk'yanchuk, M. H. Hong, and T. C. Chong, Opt. Lett. **29**, 2055 (2004).
[13] E. N. Glezer, M. Milosavljevic, L. Huang, R. J. Finlay, T.-H. Her, J. P. Callan, and E. Mazur, Opt. Lett. **21**, 2023 (1996).
[14] S. Wu, J. Serbin, and M. Gu, J. Photochem. Photobiol., A **181**, 1 (2006).
[15] J. Serbin, A. Egbert, A. Ostendorf, and B. N. Chichkov, Opt. Lett. **28**, 301 (2003).
[16] N. V. Karlov, N. A. Kirichenko, and B. S. Luk'yanchuk, *Laser Thermochemistry: Fundamentals and Applications* (Cambridge International Science, Cambridge, 1999).
[17] D. Stauffer and A. Aharony, *Introduction to Percolation Theory*, 2nd rev. ed. (Taylor & Francis, London, 1994).
[18] M. Sahimi, *Applications of Percolation Theory* (Taylor & Francis, London, 1994).
[19] M. Farsari and B. N. Chichkov, Nat. Photonics **3**, 450 (2009).
[20] S.-H. Park, D.-Y. Yang, and K.-S. Lee, Laser Photonics Rev. **3**, 1 (2009).
[21] S. Maruo and J. T. Fourkas, Laser Photonics Rev. **2**, 100 (2008).
[22] S. Juodkazis, V. Mizeikis, K. K. Seet, M. Miwa, and H. Misawa, Nanotechnology **16**, 846 (2005).
[23] G. V. Korolyov and M. Mogilevich, *Three-Dimensional Free-Radical Polymerization* (Springer, New York, 2009).
[24] P. G. De Gennes, *Polymer Physics* (Cornell University Press, Ithaca, 1979).
[25] B. Sapoval, M. Rosso, and J.-F. Gouyet, J. Phys. (France) Lett. **46**, L149 (1985).
[26] M. Rosso, J.-F. Gouyet, and B. Sapoval, Phys. Rev. Lett. **57**, 3195 (1986).
[27] J.-F. Gouyet and M. Rosso, Physica A **357**, 86 (2005).
[28] A. Desolneux and B. Sapoval, Europhys. Lett. **72**, 997 (2005).
[29] L. Balázs and J.-F. Gouyet, Physica A **217**, 319 (1995).
[30] L. Balázs, Phys. Rev. E **54**, 1183 (1996).
[31] B. Sapoval, S. B. Santra, and Ph. Barboux, Europhys. Lett. **41**, 297 (1998).
[32] J. Feder, *Fractals* (Springer, New York, 1988).
[33] V. Vdovin, A. Lonin, and S. Mensov, Tech. Phys. **46**, 853 (2001).
[34] A. Pikulin and N. Bityurin, Phys. Rev. B **75**, 195430 (2007).
[35] M. Malinauskas, A. Žukauskas, G. Bičkauskaitė, R. Gadonas, and S. Juodkazis, Opt. Express **18**, 10209 (2010).
[36] K. K. Seet, S. Juodkazis, V. Jarutis, and H. Misawa, Appl. Phys. Lett. **89**, 024106 (2006).
[37] H.-B. Sun, T. Suwa, K. Takada, R. P. Zaccaria, M.-S. Kim, K.-S. Lee, and S. Kawata, Appl. Phys. Lett. **85**, 3708 (2004).
[38] L. D. Landau and E. M. Lifshitz, *Statistical Physics*, 3rd ed. (Butterworth-Heinemann, Oxford, 1980), part 1.